Macromolecules **2007,** *40,* 3229−3237

Drastic Modification of the Dispersion State of Submicron Silica during Biaxial Deformation of Poly(ethylene terephthalate)

Stéphane Jéol,[†] Françoise Fenouillot,*,[†] Alain Rousseau,[†] Karine Masenelli-Varlot,[‡] Catherine Gauthier,[‡] and Jean-François Briois[§]

Laboratoire des Matériaux Macromoléculaires, IMP/LMM CNRS, UMR #5627, INSA-Lyon, 17 Avenue Jean Capelle, 69621 Villeurbanne cedex, France; Groupe d'Etudes de Métallurgie Physique et de Physique des Matériaux, UMR-CNRS #5510, INSA-Lyon, 7 avenue Jean Capelle, 69621 Villeurbanne cedex, France; and Tergal Industries, Rue Jules Vercruysse, BP 1, 02430 Gauchy, France

Received December 18, 2006; Revised Manuscript Received January 20, 2007

ABSTRACT: Deformation-induced modification of the dispersion state of silica nanoparticles in poly(ethylene terephthalate) (PET) has been characterized by means of transmission electron microscopy (TEM) and wide-angle X-ray diffraction (WAXD). We focused on the biaxial deformation applied at a temperature just above the glass transition temperature (110 °C), during the free stretch-blowing process of amorphous PET modified with submicron silica. The first nanocomposite studied contains 2.5 wt % of fractal aggregated pyrogenic silica. The particles are well dispersed after the polymerization of PET, but they agglomerate and orient strongly parallel to the elongation direction after biaxial deformation. They form long streams of particles (>2 μm long) regularly spaced by a distance of 50−100 nm. Interestingly, the silica organization is consistent with the hierarchical structure commonly proposed for the strain-induced crystallization of PET. The particles are rejected from the highly oriented domains induced by the strain, and their spatial organization reveals the superstructure. The second nanocomposite contains 5% of spherical silica with a diameter of 20 nm. Its behavior is drastically different. The silica also forms streams of particles (1−2 μm long); however, the streams are oriented perpendicular to the elongation direction, and that is hardly compatible with the presence of a microfibrillar structure. We assume that this unexpected orientation is produced by the extended growth of mesophases and crystallites perpendicular to the orientation and that stacked lamellae are formed rather than microfibrils.

1. Introduction

Poly(ethylene terephthalate) (PET) is one of the most important engineering polymers, and its leader position can be explained by its excellent mechanical and gas barrier properties, low color, and high transparency. Considering that it is commercialized at the price of a commodity polymer, it is a serious challenge to enhance PET properties. One possibility consists in modifying the polymer with various kinds of submicron-sized inorganic fillers. As an example, modified nanoclays added in PET either in a twin-screw extruder or directly during the synthesis of the polymer allow to reduce the permeability to carbon dioxide and to increase thermomechanical properties.[1−6] Other particles like silica (SiO_2), titanium dioxide (TiO_2), calcium carbonate ($CaCO_3$), barium sulfate ($BaSO_4$), talc, and carbon nanotubes have been tested,[7−12] and by contrast with the difficulties encountered to break nanoparticle agglomerates in polyolefins, good dispersions are generally achieved in PET. Besides, the above-cited studies present extensive characterization of the state of dispersion obtained. However, if the quality of the dispersion is a key for property improvement, a controlled dispersion must be obtained not only on the initial nanocomposite after its preparation but also on the final object. PET is exploited in fibers, films, and bottles produced by uniaxial or biaxial stretching. This technique implies that unoriented amorphous PET is heated above its glass transition temperature (T_g) and stretched so that crystallization is induced by the orientation. Such processing have major effects on several end-use properties like permeability, transparency, rigidity that clearly depends on the crystalline volume fraction, the orientation and size of the crystals, and the degree of elongation of the macromolecules. For nanocomposites, an essential issue is to determine whether the presence of the particles alters the development of the crystalline structure; and how dispersed rigid nanoparticles can be affected by the strong deformation experienced by the polymer.

Whereas considerable effort has been made to characterize and interpret the strain-induced crystallization of neat PET, very few studies were devoted to filled PET[13−15] and even less to PET filled with submicron particles.[16] The aim of this study was thus to characterize the dispersion of two types of submicron silicas in PET nanocomposites synthesized and subsequently processed by injection-molding followed by free stretch-blowing. Since we were particularly interested in the biaxial stretching step, the morphologies observed have been compared and discussed in light of the existing structural models proposed to describe strain-induced crystallization of PET.

2. Experimental Section

2.1. Synthesis of the Nanocomposites. Two types of silica have been used: a pyrogenic fractal aggregated silica (HDKT30 from Wacker Chemie) and a precipitated spherical silica (DP5820 from Nyacol Nano Technologies, Inc.). The first was a solid that was dispersed in ethylene glycol (EG) before introduction in the reactor (15 wt % silica in EG); its specific area was 300 m^2/g. The second was a colloidal suspension of 30 wt % of silica spherical particles with an average diameter of 20 nm, in ethylene glycol. The presence of negative charges at the surface of the silica particles (SiO^-Na^+) stabilizes the dispersion by electrostatic repulsions.

The fractal aggregated silica content of the PET was 2.5 wt %, and the spherical silica content was 5 wt %. In the rest of the article,

---

* Corresponding author. E-mail: francoise.fenouillot@insa-lyon.fr.

[†] IMP/LMM CNRS, UMR #5627.

[‡] UMR-CNRS #5510.

[§] Tergal Industries.

10.1021/ma062886i CCC: $37.00

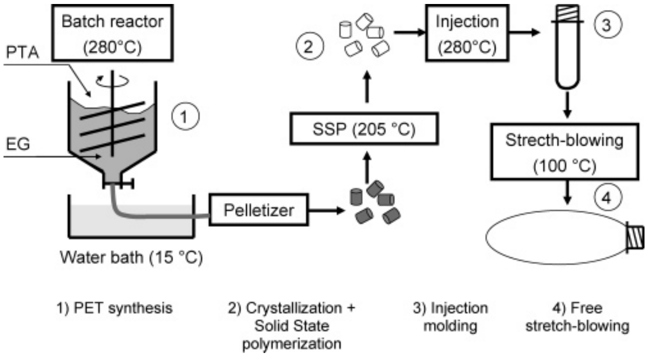

Figure 1. Elaboration steps of a PET bottle: (1) PET synthesis, (2) solid-state polymerization (SSP), (3) injection molding, (4) free stretch-blowing.

the terms "fractal silica" and "spherical silica" refer to the different types of fillers.

Terephthalic acid (PTA), isophthalic acid (AIP), ethylene glycol (EG), and antimony trioxide (Sb_2O_3) were supplied by Tergal Industries (Gauchy, France). The polymerization in a 7.5 L batch reactor included two steps: the esterification reaction between terephthalic acid (PTA) and ethylene glycol (EG) in the presence or not of the silica particles, followed by a transreaction of the ester catalyzed by antimony (Sb_2O_3). The reactor is stirred with a helical impeller rotating at 45 rpm. The PET/silica was finally extruded out of the reactor and quenched in cold water to obtain amorphous pellets. After heating at 130 °C for 3 h to crystallize the PET/silica, the solid-state polycondensation (SSP) was done at 205 °C under a N_2 stream for 16 h to increase the molecular weight of the chains.

2.2. Injection-Molding of the Preforms. After the SSP, the pellets were dried under vacuum at 130 °C for 16 h to avoid hydrolytic degradation during injection-molding. They were injected in a mold cooled at 11 °C to form amorphous preforms. The preform thickness was equal to 3 mm. The screw speed of the plastification unit was set at 200 rpm, generating a shear rate higher than 100 s^{-1}.

2.3. Stretch-Blowing of the Preforms. The amorphous preforms were submitted to a stretch-blowing process without mold called free stretch-blowing process. The preform was heated at 100 °C, above T_g (80 °C) but below the cold crystallization temperature ($T_{cc} = 130$ °C), so that spherolitic crystallization is avoided. The free stretch-blowing process is divided into two steps: a uniaxial elongation of the preform in the longitudinal direction imposed by the stretcher, at a speed of 750 mm/s followed by a biaxial elongation in both the longitudinal and transverse directions imposed by a pressure of nitrogen gas set at 7 bar for 0.2 s. During this stage, the pressure initiates the formation of a bubble that propagates from the top of the uniaxially stretched preform toward the bottom; this generates a biaxial elongation of the PET along the longitudinal and transverse directions. The obtained container is cooled using compressed air. During the stretch-blowing process, the thickness of the preform decreases from 3 to 0.3 mm in 0.2 s. The global draw ratios were $\lambda_L = 3.3$ in the longitudinal direction and $\lambda_T = 3.5$ in transverse direction. A diagram summarizing the whole process is given in Figure 1, and the stretching directions and axis are described in Figure 2.

2.4. Nanocomposite Characterization. *Reduced Viscosity (IV).* The polymer molecular weights are estimated by measuring the reduced viscosity (IV) at 25 °C for a 0.5 wt % solution of polymer in a phenol/*o*-dichlorobenzene 50/50 wt % mixture.

Thermal Properties. The thermal properties of the PET nanocomposite and neat PET are examined with a DSC7 Perkin-Elmer thermal analyzer. Enthalpy and temperature are calibrated with indium under a nitrogen atmosphere. All samples are submitted to the following cycle: first heating 35−290 °C (+10 °C/min), isotherm at 290 °C (5 min), cooling 290−35 °C (−10 °C/min), second heating 35−290 °C (+10 °C/min). The melting temperature, T_m (first heating), and cold crystallization temperature, T_{cc} (first heating), crystallization from the melt, are measured at the maximum of the peak. The melting enthalpy for a whole crystallized PET $\Delta H_{m-crystal}$ is taken equal to 117.6 J g^{-1}.[17] The degree of crystallinity, X_c, is evaluated by the following equation with φ_S, the mass fraction of silica:

$$X_c = \frac{1}{1-\varphi_S}\frac{\Delta H_m - \Delta H_{cc}}{\Delta H_{m-crystal}} \times 100 \qquad (1)$$

Morphology. The samples were cut with a 45° diamond knife at room temperature on an ultramicrotome Ultracut Reichert S. The speed was set to 1.5 mm s^{-1} and the thickness to 50 nm. The sections were then deposited on a 400 mesh copper grid. As far as the bottles are concerned, the samples were first embedded in an epoxy resin (Epofix). Moreover, thin sections were taken in the middle of the bottle and cut either perpendicular or parallel to the bottle axis (Figure 2). The transmission electron microscopy (TEM) observations are carried out on a JEOL 200 CX microscope (LaB_6 filament, accelerating voltage 200 kV). The images were acquired in the bright field mode. Knowing that the orientation and overall morphology may be different depending on the location in the samples, we made microscopic observations all across the preform and bottle walls. The images selected and presented further represent what we observed all across the sample

Wide-Angle X-ray Diffraction (WAXD). Wide-angle X-ray scattering (WAXS) was carried out on the D2AM beamline of the European Synchrotron Radiation Facility (ESRF). The wavelength of the X-rays was 0.54 Å, and the specimen−camera length was set to 240 mm. The two-dimensional (2D) WAXS patterns were recorded with a CCD camera (Princeton Instruments).

PET crystallizes according to a monoclinic unit, whose parameters are equal to $a = 4.56$ Å, $b = 5.94$ Å, $c = 10.75$ Å, $\alpha = 98.5°$, $\beta = 118°$, and $\gamma = 112°$.[18] In order to obtain a 3-dimensional view of the orientation of the crystal unit of PET, the 2-dimensional WAXS patterns along three different directions have to be considered. According to the axes defined on Figure 2, 2D WAXS patterns were acquired with the X-ray beam being perpendicular either to the (θ r) or to the (θ Z) or to the (rZ) plane of the bottle. Moreover, one of the ways to quantify the orientation of the crystal unit is to draw a diagram called the Wilchinsky diagram. The detailed procedure is described elsewhere by Bafna et al.[19]

3. Results and Discussion

The properties of the nanocomposites are presented in Table 1. The reduced viscosities measured for PET, PET/2.5% fractal silica, and PET/5% spherical silica are respectively 0.78, 0.73, and 0.69 dL g^{-1}, which correspond to a number-average molecular weight of 18 300, 16 700, and 15 600 g/mol.[20] The polydispersity index generally obtained is between 1.95 and 2.05.

The global process was then considered, and the nanoparticles dispersion has been characterized at each step: after the synthesis, after the injection-molding, and finally after the biaxial elongation.

3.1. Dispersion of Silica in PET after Synthesis and Solid-State Polycondensation. The observation of the TEM images recorded on the amorphous pellets obtained after the synthesis reveals a homogeneous dispersion of almost perfectly individualized spherical silica nanoparticules in PET (Figure 3 a). The interparticle distance (distances between the centers of two neighboring particles) is estimated to be 41 nm. The experimental mean distance corresponds well with the 39 nm calculated with the following equation, where r is the radius of the particle and ϕ the volume fraction of silica.

$$d = \left(\frac{4\pi\sqrt{2}}{3\phi}\right)^{1/3} r \qquad (2)$$

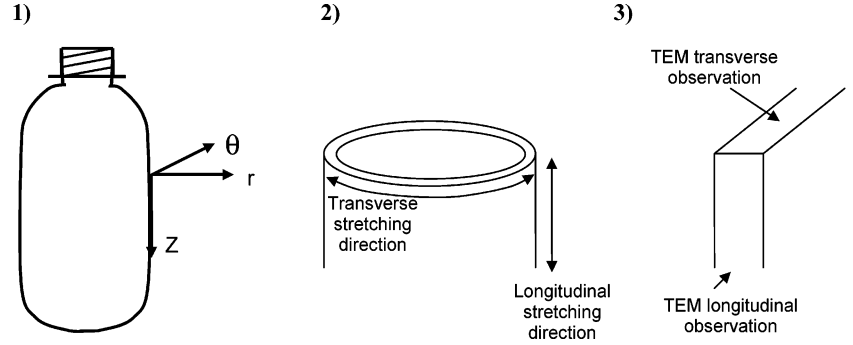

Figure 2. (1) Bottle geometry and coordinate system. *Z*: longitudinal direction; *θ*: transverse or ortho-radial direction; *r*: radial direction. (2) Elongation directions during the stretch-blowing process. (3) Observation directions (*rθ* and *rZ* planes).

Table 1. Reduced Viscosity and Thermal Properties of the PET and PET/Silica[a]

sample	reduced viscosity (dL/g)	T_{cc} (°C)	ΔH_{cc} (J g^{-1})	T_m (°C)	ΔH_m (J g^{-1})	degree of crystallinity (wt %)
amorphous PET after synthesis	0.78	131	43	247	50.3	6.0
PET/5% spherical SiO_2						
amorphous after synthesis	0.69	130	45	246	51	5
crystalline after SSP	0.84			245	71	60
preform		126	41	247	48	5
uniaxially stretched perform		121	39	245	48	8
bottle		98	6	245	62	48
PET/2.5% fractal SiO_2						
amorphous, after synthesis	0.73	132	44	248	50	5
bottle		98	7	248	65	50

[a] T_{cc}, ΔH_{cc}: cold crystallization temperature and enthalpy; T_m, ΔH_m: melting temperature and enthalpy.

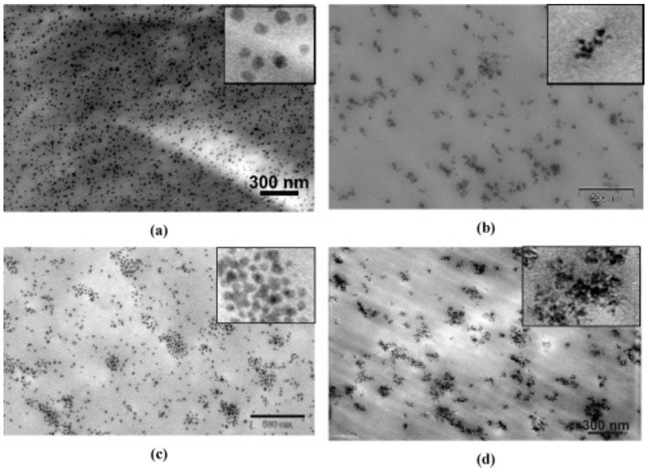

Figure 3. TEM micrographs of the amorphous PET nanocomposites: (a) PET/5% spherical silica after synthesis, (b) PET/ 2.5% fractal silica after synthesis, (c) PET/5% spherical silica after injection-molding, and (d) PET/2.5% fractal silica after injection molding. Inserts are zoomed regions of the images (×4 to ×8). The silica particles appear in black.

In other words, the excellent initial dispersion of silica in ethylene glycol is preserved during the PET synthesis.

The spherical silica consists of simple individualized spherical silica particles, in contrast to the structure of the fractal silica which is more complex. For the latter, the term "particle" designates an aggregate of primary particles with a diameter of 9 nm. The aggregate cannot be broken by any classical dispersion technique. In this work, the term "aggregate" refers to this specific structure while the term "agglomerate" refers to a group of aggregates. A view of an aggregate is shown in Figure 3b. The fractal silica is also well dispersed, but some agglomerates are present (Figure 3b). This indicates that the shear rate induced by the rotation of the impeller was not sufficient to break the agglomerates present in the initial silica dispersion prepared by ourselves. This dispersion in ethylene glycol was slightly turbid, indicating the presence of entities that diffuse light.

The following crystallization and SSP treatments result in a high degree of crystallinity of the PET, 60% determined by calorimetry (Table 1). As expected, the crystalline PET/silica nanocomposite has the same morphology as the amorphous one since the thermal treatment was done at the solid state. Note that the term "morphology" refers to the quality of the silica dispersion and not to the crystalline microstructure.

3.2. Dispersion of Silica after Injection-Molding. After the synthesis and SSP, the PET/silica is injection-molded in order to obtain the preform. We briefly remind the features of this process in order to help the understanding. The pellets are plasticized inside the barrel of the injection machine. When the polymer has totally melted, it is injected in the cold mold to quench the part and to avoid crystallization. The low degree of crystallinity of the PET was confirmed by DSC and found to be 5%.

For both the spherical and fractal silicas, the TEM pictures show a significant agglomeration of the particles (Figure 3c,d). In the spherical silica agglomerates (see zoom in Figure 3c), each silica particle is spaced from the others by a distance ranging from 0 to ~10 nm. The morphology is isotropic as was confirmed by the TEM observations in the perpendicular direction (not shown here). The size of the agglomerates ranges from 100 to 500 nm. To interpret this morphology change, it is useful to point out some of the mechanisms involved in particles agglomeration in a flow field. Forming agglomerates requires the approach of particles that is often quantified by the probability of occurrence of a collision. This probability is proportional to the shear rate (laminar flow) and to the volume fraction of particles.[21] Second, to form an agglomerate, the particles must come in contact; this requires that they are given sufficient energy (thermal, mechanical) to drain the molten polymer layer in between the particles and also to overcome the energy barrier that prevents the contact, the van der Waals attractive forces becoming predominant at short distance.[22] If the energy brought by the shear is higher than the barrier energy, the silica particles agglomerate.

To conclude on the morphologies obtained after the synthesis, the observation of the TEM images on the amorphous pellets shows a quasi-perfect separation of silica particles from each other, which means that the low speed of the helical stirrer does not produce sufficient stresses to drain the interparticle polymer layer and overcome the barrier energy required to force silica particles to agglomerate. For fractal silica, the shear is too low to break the initial agglomerates present in the initial dispersion introduced into the reactor. In contrast, the high shear rate experienced during injection-molding generates a force able to push the particles in contact; the important aspect here is that the injection-molding step causes a significant alteration of the excellent initial silica dispersion.

3.3. Dispersion of Silica after Uniaxial Stretching of the Preform. During the first uniaxial stretching the length of the preform increases while the diameter remains almost unchanged. We define the draw ratio λ_{L1} as the ratio of the uniaxial stretched length over the initial length of the preform. For our operating conditions, $\lambda_{L1} = 1.5$. According to numerous studies on uniaxial stretching of amorphous PET, a minimum stretching (that depends on strain rate, temperature, molecular weight) is necessary to cause some orientation of the PET and further induce crystallization.[23−28] When the stretching ratio is too low (<2), the material remains amorphous with highly oriented zones containing chains in their trans configuration and less oriented zones; this structure crystallizes at low rate. Our thermal measurements confirm that feature since a degree of crystallinity of only 8% is found for the uniaxially stretched preform, which corresponds to an increase of 3% compared to the degree of crystallinity of the unstretched preform (Table 1).

The preform wall was examined in two directions: longitudinal and transverse. The TEM observations are not presented here because they show that the dispersions of the silica in both longitudinal and transverse directions, for unstretched and uniaxially stretched preforms, are similar, with the presence of isotropic agglomerates of particles. Therefore, we conclude that the uniaxial stretching step has no significant influence on the dispersion.

3.4. Dispersion of Silica after the Biaxial Stretching. After the preform is elongated, the air pressure causes the inflation of a "bubble" at the top of the preform. The propagation of the bubble generates a biaxial deformation of the PET with draw ratios $\lambda_{L2} = 2.3$ in the longitudinal direction (Z) and $\lambda_T = 3.5$ in the transverse direction (θ). The bottle geometry is defined in Figure 2, we assign Z to the axial, θ to the orthoradial (or transverse), and r to the radial or out-of-plane directions. The global draw ratios are $\lambda_L = \lambda_{L2}\lambda_{L1} = 3.3$ in the longitudinal direction and $\lambda_T = 3.5$ in transverse direction. According to the value of the draw ratios, a major chain orientation is expected along the θ axis and to a less extent along the Z axis.

In the same way as the preform, the microscopic observations on the bottle wall are made, in two directions called longitudinal (view of the rZ plane) and transverse directions (view of the $r\theta$ plane) (Figure 2).

3.4.1. Orientation of the Crystal Units of PET. The monoclinic crystal unit of PET leads to several diffraction peaks. Three different configurations were studied, depending on the respective orientation of the bottle specimen and the X-ray beam. The corresponding WAXS 2D patterns of the PET/5% spherical SiO_2 bottle are displayed in Figure 4. Similar 2D patterns were obtained with the pristine PET and the PET/2.5% fractal SiO_2 bottles (not displayed).

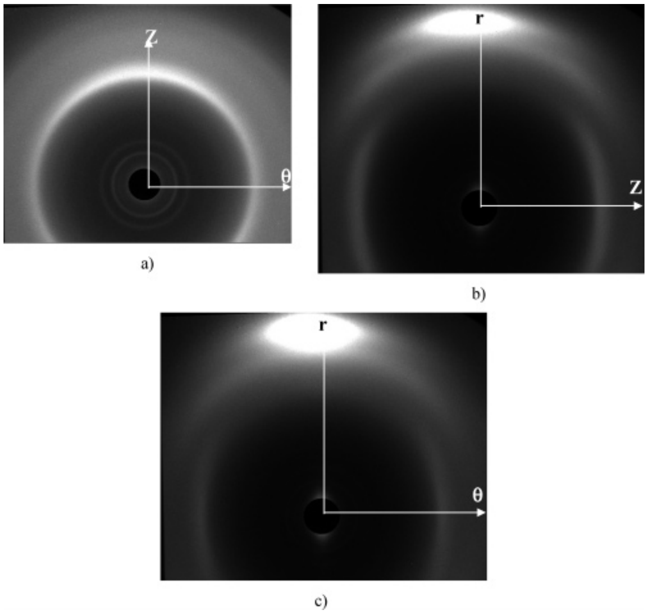

Figure 4. WAXS 2D patterns of the PET/2.5% fractal SiO_2 bottle, with three different configurations, the X-ray beam being perpendicular to (a) the (θZ) plane, (b) the (rZ) plane, and (c) the (θr) plane of the bottle.

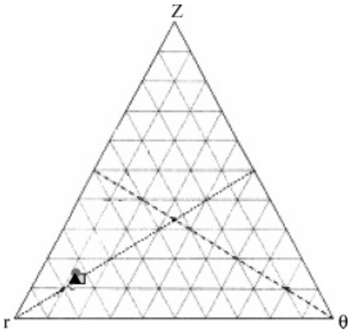

Figure 5. Wilchinsky diagram showing the orientation of the a vector of the PET monoclinic unit in the pristine PET bottle (triangle), in the PET/5% spherical SiO_2 bottle (circle), and in the PET/2.5% fractal SiO_2 bottle (square).

When looking at a bottle with the (θZ) plane perpendicular to the X-ray beam (Figure 4a), rings are observed. The most intense ring, observed for a scattering vector q of about 1.2, is due to the diffraction of the (001) and (010) planes of the PET monoclinic unit. Unfortunately, this ring is due to the diffraction of several planes, and it is not possible to go further. The two other configurations (Figure 4b,c) lead to the presence of very intense spots at $q = 1.71$, which are due to the diffraction of the (100) plane. It is possible to quantify the orientation of the (100) plane from these 2D patterns, through the Wilchinsky diagram.[19] Basically, the Wilchinsky diagram is a ternary diagram of orientation. If a plane is not oriented in the sample, the corresponding point will be located on the diagram at the intersection of the three bisectors. On the contrary, if a plane is perfectly oriented, for example with its normal vector parallel to the Z direction, the corresponding point will be located at the Z summit of the Wilchinsky triangle.

Figure 5 represents the Wilchinsky diagram for the orientation of the (100) plane of the PET monoclinic unit. The point of the pristine PET bottle is relatively close to the r summit of the triangle, which means that the vector normal to the (100) plane (the a vector of the monoclinic unit) is well aligned in the r

direction. Moreover, this point is located on the bisector, which means that the θ and Z directions play similar roles. This is in agreement with the presence of rings in Figure 4a. It is concluded that the *b* and *c* vectors of the PET monoclinic unit are orthotropically oriented in the (θZ) plane of the bottle. This implies that the *a* vector is mainly oriented along the *r* direction of the bottle, its nonperfect orientation being due to the fact that the angles in the PET crystal unit are not equal to 90°.

Moreover, no difference can be found in the orientation of the (100) plane in the pristine PET, PET/5% fractal SiO_2, and PET/2.5% spherical SiO_2 bottles. It can thus be concluded that the presence of SiO_2 does not affect the orientation of the PET crystal unit in the bottle.

3.4.2. Dispersion of Fractal Silica after Biaxial Stretching. First we should emphasize again that we designate the dispersion state of the silica by the term “morphology”, whereas the term “structure” or “microstructure” refers to the PET crystalline organization.

The morphology of the PET/fractal silica is seen in the two directions of observation as lines or streams of silica particles, 0.3−1 μm long and oriented along the two directions of deformation (Figure 6). The literature devoted to the organization of inorganic nanofillers during deformation is not abundant, and at this point we must turn toward studies about polymer blends. The morphology may be understood if we consider how heterogeneities like nodules of an immiscible polymer deform in a polymer matrix submitted to elongation. As an example, a fibrillar dispersed polymer phase is obtained by the elongation of a polymer blend at the die exit of an extruder.[29,30] Also, with PET as the matrix, the biaxial elongation of a PET/poly(*m*-xylylene adipamide) blend deforms the polyamide spherical domains into high aspect ratio platelets.[31] Here, the agglomerates of fractal silica formed after the injection molding of the preform behave like a dispersed polymer phase and are elongated in the θ and Z directions.

More interestingly, we note that the silica streams are regularly spaced, at an average distance ranging from 50 to 150 nm, and that absolutely no silica is found in the regions between the streams. This observation leads us to the question of the relations between the state of dispersion of the silica particles and the microstructure of PET. The structural development by uniaxial deformation above T_g of quenched amorphous PET has been studied because it is involved in several industrial shaping operations and is known to influence strongly the end-use properties (modulus, transparency, permeability). Recent reviews give an overview of the flow-induced crystallization process.[32,33] It is now well-established that flow (shear, stretching, or drawing) considerably affects the structural evolution of the polymer and its kinetics. In PET, uniaxial solicitation promotes the stretching and orientation of the molecular chains, and nematic and smectic phases can appear, especially below T_g. Above T_g, these mesophases can also exist provided that the draw rate is high enough and the temperature not too high (<125 °C).[34−37] Depending on the draw rate, temperature, and the existence of an annealing step, subsequent crystallization can develop accompanied or not by a tilting of the *c*-axis of the triclinic unit cell.[38] In polypropylene, the mesophase can act as nucleating sites for crystallization. In PET, the mesophase

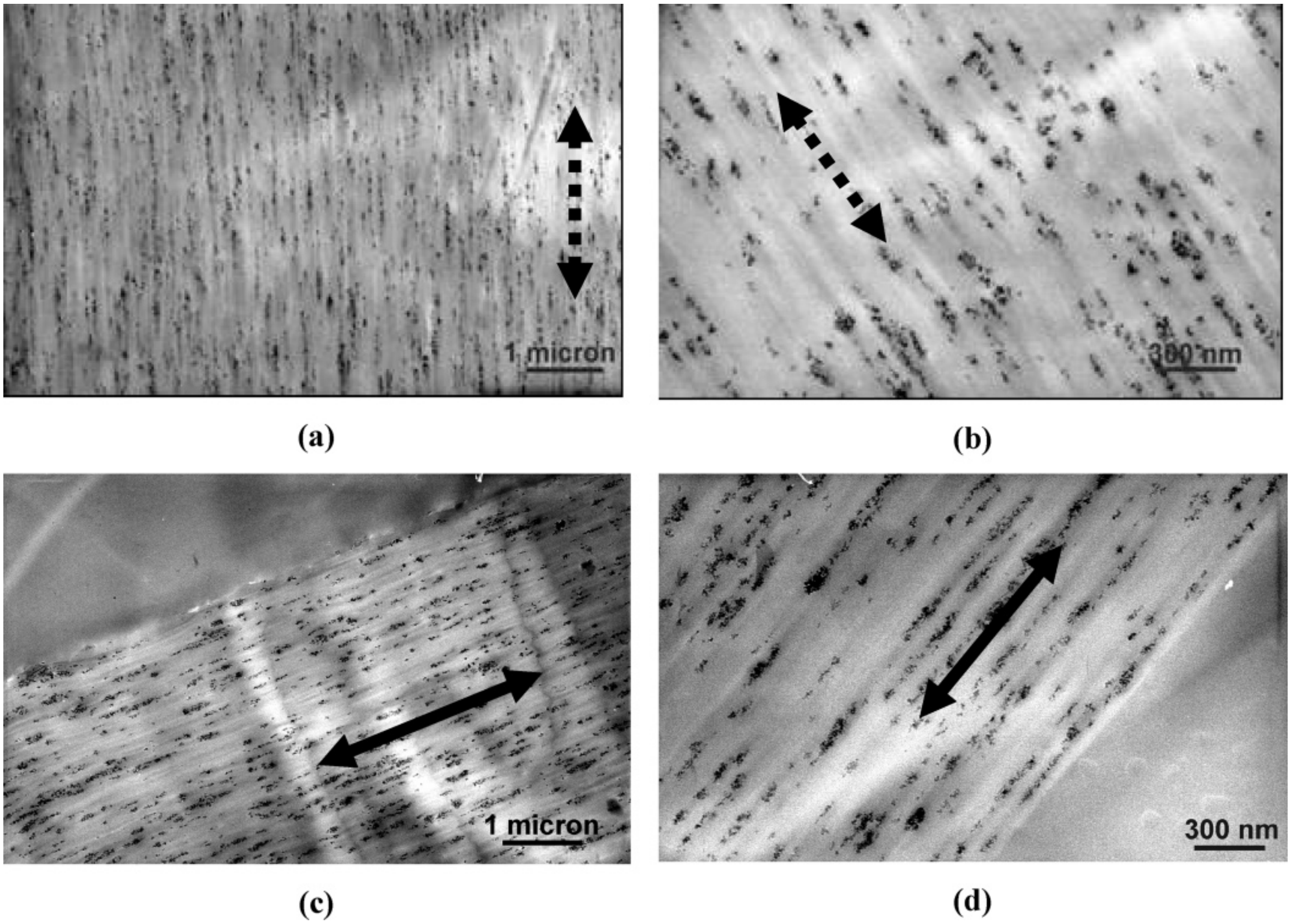

Figure 6. TEM micrographs of PET/2.5% fractal silica after stretch-blowing (a, b) longitudinal observation (*rZ* plane). The dotted arrow indicates the longitudinal elongation direction. (c, d) Transverse observation (*r*θ plane). The black arrow indicates transverse elongation direction.

is supposed to behave like a template or precursor whose ordering facilitates the crystallization, and the strain-induced crystallization occurs mainly in the mesophase region. The crystallization process is accelerated so much by the existing molecular orientation that no crystallization directly from the amorphous region is observed. Also at high strain rates, the crystallization process does not begin until the end of the stretching, and it is so fast (1−100 ms) that it may take place even during deep quenching of the sample.[23,27,36] As an example, Blundell[27] and Mahendrasingam[26] measure 0% crystallinity of PET at the end of draw at a draw rate of 12.8 s^{-1}, a temperature of 90 °C, and a draw ratio of 3.5. At 90 °C, he finds that above a draw rate of 1 s^{-1} the onset of crystallization coincides with the end of the deformation process; that is, crystallization starts as soon as the deformation stops. Although the above features are now accepted and demonstrated, there exist very few indications on the structure of stretched PET on a larger scale. In other words, in most of the published works the thickness and the spacing of smectic layers (and subsequent lamellae) are measured, but it is difficult to get actual data in terms of dimensions of the superstructures and accordingly obtain a global picture of how these entities are organized. This is probably due to the high complexity of the experiments and interpretations, especially when the formation of superstructures is followed in-situ by coupled techniques as achieved by authors in recent works. We emphasize the importance of a quantification of the dimensions since we believe that in our nanocomposite the fractal silica particles are rejected from the highly oriented mesophase and crystallites toward the less oriented amorphous phase. Thus, it is crucial to determine whether the shape and size of the oriented zones are consistent with the present silica organization. As an example, in the case of uniaxial solicitation, different studies converge to assert that the induced structure consists in microfibrils aligned parallel to the stretching direction and surrounded by more or less oriented amorphous phase. The microfibrils contain tilted lamellae and stretched chains.[25,39−41] Kawakami and co workers investigate the phase transition during uniaxial deformation (at 80, 90, and 100 °C) by simultaneous 2D small-angle X-ray scattering (SAXS) and wide-angle X-ray diffraction (WAXD) using synchrotron radiation.[39,40] They propose a description of phase transition and structure development pathways that will not be detailed here. Only the final structure model is outlined. They identify fibrils with a diameter ranging from 20 to 60 nm and a length of several hundred nanometers. If the morphology presented in Figure 6c,d is considered in light of these data, we note that the distance between the particle streams and their length are consistent with the sizes of fibrils proposed by Kawakami. However, it is necessary to be cautious and to remember that these works are carried out at rates of deformation lower than those encountered here. As an example, our operating conditions impose deformation at 750 mm/min while the deformation rate imposed by Kawakami was 5 mm/min. In the experiments of Kawakami, crystals are formed at the end of the process and are revealed by the X-ray diffraction pattern. At 110 °C and a draw rate close to 10 s^{-1}, Mahendrasingam also observes that the crystallization starts during the deformation stage and is achieved at the end of the process.[42] On the

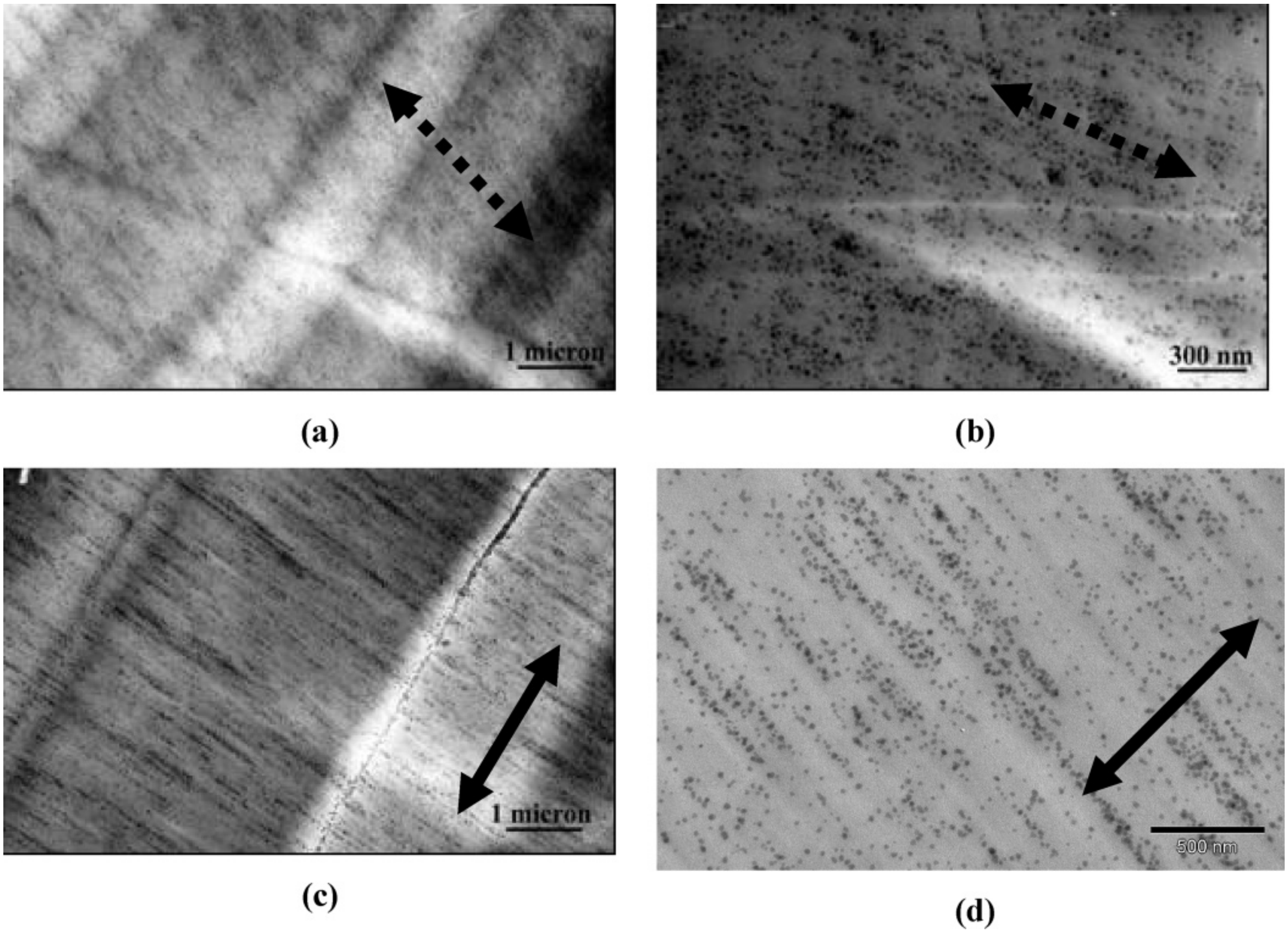

Figure 7. TEM micrographs of PET/5% spherical silica after stretch blowing (a, b) longitudinal observation (*rZ* plane). The dotted arrow indicates the longitudinal elongation direction. (c, d) Transverse observation ($r\theta$ plane). The black arrow indicates transverse elongation direction.

other hand, several authors believe that only nematic and/or smectic phases are formed and that crystals appear only upon a relaxation mechanism when the deformation is interrupted.[23,43] Our process of free-blowing is run at 30 s^{-1} strain rate and ends by a fast cooling step imposed by an external air-blowing, but probably it is not fast enough to quench the mesophase since crystals are formed.

To summarize, we believe that the fractal silica particles are rejected from the oriented and crystallized zones of the PET. They organize in the shape of flat agglomerates (platelets) elongated in the θZ plane that corresponds to the directions of deformation. An interesting aspect is that the silica morphology reveals the shape and size of the oriented superstructures of PET. We cannot call them microfibrils since the orientation is biaxial instead of uniaxial, but their thickness (50−150 nm) and length (1 μm) correspond well to the data estimated by Kawakami despite the application of a much higher strain rate.

3.4.3. Dispersion of Spherical Silica after Biaxial Stretching. In the longitudinal view (rZ plane) a weak orientation of the silica agglomerates is observed parallel to the axial stretch direction (Figure 7a,b). The situation is totally different when looking at the transverse section ($r\theta$ plane) of the bottle wall presented in Figure 7c,d. Surprisingly, the orientation of the silica agglomerates is perpendicular to the main stretching direction (transverse). The agglomerates of particles are strongly elongated in the shape of ellipses, with a length around 1 μm and a thickness ranging between 50 and 150 nm. The ellipses are supposed to be the result of the deformation of the initial silica agglomerates found in the amorphous preform; however, they have been deformed following a 90° angle compared to the transverse elongation axis. This feature was quite unexpected, and the experiment was repeated to confirm it. The stretching process by itself cannot explain the deformation of silica agglomerates perpendicular to the stretching direction. Also, in the framework of the structural models of strain-induced crystallization discussed previously, it is difficult to imagine how a fibrillar superstructure (oriented parallel to the elongation) can fit the morphology presented in Figure 7c,d. Actually, the only structures that may develop perpendicular to the elongation direction are the smectic layers and the lamellae. If we first consider the case of the smectic layers, it is not said in the literature whether they are able to grow extensively in a direction perpendicular to the stretching direction or if their size is small. This is of importance since it appears that the elongated silica particles agglomerates are about 500−1000 nm long. On the other hand, the structures known to develop in an extended way (0.5−1 μm) perpendicular to the elongation direction are lamellae as observed in shish-kebabs.[33] Shish-kebabs consist of a central fiber (shish) from the surface of which crystals develop (kebab). Shish-kebabs are generally recognized in high molecular weight polymers (e.g., polyethylene, polypropylene) and rarely in aromatic polyesters since their molecular weight is much lower. Shish-kebabs were nicely visualized in ultrahigh molecular weight polyethylene (UHMWPE) by selectively extracting the amorphous phase and observing the structures by field emission scanning electron microscopy.[44] The shish-kebabs are long (1−10 μm); the average diameter of the shish is 10 nm to a few tens of nanometers, and the distance between neighboring kebabs is 30−100 nm. The adjacent kebabs are sometimes connected so that their plane can develop to several hundreds of nanometers. The existence of shish-kebab in PET is not mentioned, but recently, Li and de Jeu visualized by AFM long lamellae (several hundred nanometers) oriented perpendicular to the flow direction in a poly(butylene terephthalate) (PBT) crystallized under shear at 198 °C and proposed a microshish model.[45] Yishioka et al. observed for the first time by TEM the formation of long stacked lamellar structure during the uniaxial orientation of thin films of PBT and PEN but not in PET.[46,47] The great advantage of a direct visualization is that it is possible to measure the dimension of the structures. In PBT, the authors report that stacked-lamellar structures of 1 μm long (or more) are formed along the shearing direction. They also give the length of the lamellae that is estimated at 100−200 nm. Although these data concern UHMWPE, PBT, and PEN, it is interesting to have the orders of magnitude in mind to note that the size and shape of these structures are compatible with the morphology of the silica that we observe.

3.5. Discussion. Once again, the basic starting point is that both types of silica are rejected from crystals and highly oriented PET phase. On the one hand, the organization of the fractal silica reveals a structure similar to microfibrils, except that we have a biaxial geometry of the structure. The microfibrils and the flat agglomerates of silica particles are oriented in the θr plane, corresponding to the directions of elongation. By contrast, for spherical silica we hardly see how microfibrils can coexist with silica agglomerates strongly oriented perpendicular to the main elongation direction. It seems reasonable to say that the shish-kebab or stacked lamellae structure is more likely to match the silica arrangement, both in terms of orientation and dimensions of the agglomerates. We hypothesize that the agglomerates present before blowing are deformed by the growth of structures similar to kebabs or stacked lamellae perpendicular to the stretching axis. In that way ellipsoidal silica agglomerates are generated. We propose a schematic view of the structure that we imagine in Figure 8 as well as a comparison between the morphologies seen with spherical and fractal silica at the same scale and with the same orientation of the stretching direction. TEM performed on stained samples could have been an efficient technique to confirm the morphologies and structure.[48] Unfortunately, we could not obtain enough contrast between the PET crystalline and amorphous phases, which might suggest that the strain-induced crystallites are highly defective compared to crystallites obtained by thermal crystallization.

The above interpretations involve that the PET superstructure is different depending on the type of nanofiller. In other words, PET chains submitted to deformation do not behave in the same way depending on whether fractal or spherical silica is present. The superstructure generally observed for stretched PET being microfibrillar, an important question is to determine why spherical silica alters the classical development of the crystalline superstructure, favoring the growth of extended superstructures at 90° angle compared to the θ and Z elongation directions. This is a difficult point and the only published study in this field to our knowledge is the work of Taniguchi, who proved that 0.35 wt % TiO_2 with a diameter of 0.1 μm retards strain hardening, producing films with lower crystallinity and orientation levels.[16] The particles act as “antinucleating” agents during deformation. In the domain of thermal-induced crystallization, Waddon and Nitta report that spherical silica decreases the spherulite growth rate of respectively polyoxyethylene and polypropylene during quiescent crystallization.[49,50] They propose that the mobility of the crystallizing units is reduced by the spatial confinement between particles. In PP, the spherulite growth rate is reduced by a factor 2−4 by the presence of 5 wt % 25 μm diameter silica with the interparticle distance ranging from 100 to 50 nm. The situations described in the three studies cited here are not exactly similar to ours, but they allow to sketch

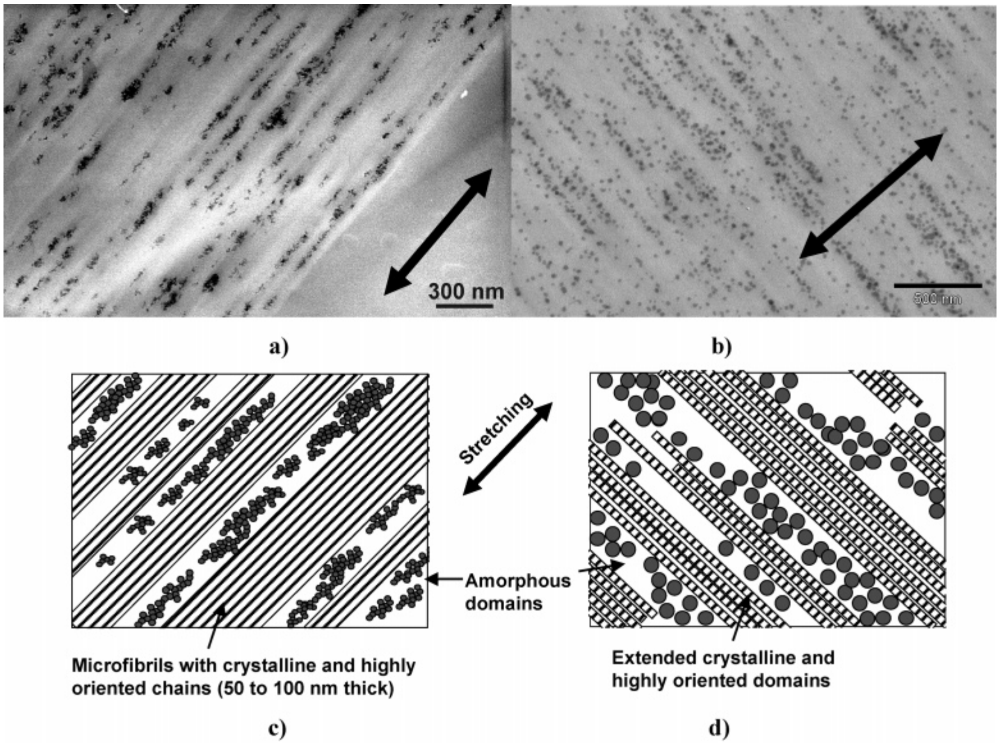

Figure 8. Comparison of the morphology of PET/2.5% fractal silica and PET/5% spherical silica after biaxial stretching (a and b, respectively) and schematic representation of the morphology (c and d). View of the $r\theta$ plane. The scale is the same for the two pictures, and the direction of the stretching is the same for all views.

out propositions of interpretation. Indeed, the spatial confinement is even more drastic inside the agglomerates of particles depicted in Figure 3c (see zoomed view). The distance between adjacent silica spheres is less than 10 nm, and it is very likely that PET chains present inside the agglomerates do not have the possibility to orient to the same extent as those situated outside. If we suppose that PET does not crystallize inside the agglomerates, it can explain that these zones remain sufficiently mobile to be deformed by the growth of the crystalline morphology.

4. Conclusion

Before concluding, one should bear in mind that the understanding of the evolution of the dispersion of nanofillers in relation to the microstructure of the PET is of great importance for end-use properties. As a practical example, the presence of agglomerates of particles leads to diffusion of light and loss of transparency of the material. It may also greatly influence the permeability properties since it is well-known that tortuosity of the gas pass is an important parameter to consider in this field.

In this context, the results presented here can be summarized as follows:

- The dispersion state of two types of submicron silica (spherical and fractal) was found to be excellent after the in-situ synthesis of the PET nanocomposites. Especially, the spherical particles are well individualized, and no agglomerates are observed. Some agglomeration is found with the fractal silica, but it is due to the imperfect initial dispersion in the ethylene glycol monomer and the low intensity stirring that was not able to break the remaining agglomerates.
- The injection-molding stage has a significant impact on the morphology; the high shear is able to accelerate the draining of the molten polymer layer between the colliding particles and overcome their energy barrier. Therefore, it leads to the formation of isotropic agglomerates for both types of silica.
- Finally, the biaxial elongation imposed during the free-blowing process strongly modifies the dispersion state of the silica. The isotropic agglomerates of particles are elongated parallel or perpendicular to the deformation directions depending on the type of nanofiller, respectively fractal or spherical. Whereas the organization of the fractal silica is consistent with the microfibrillar structure often initiated by strain-induced crystallization of PET, the spherical silica organization is not. We propose that in the presence of spherical silica particles long stacks of lamellae (and mesophase) are formed separated by wide amorphous less oriented domains where the particles tend to be situated. The question of the crystallization model of PET is much debated, and we are aware that the stacked lamellae model is not the most currently admitted in drawn PET; however, it is able to explain that the particles agglomerates are elongated at a 90° angle compared to the stretching direction. Indeed, a direct observation may help to provide a view of the crystalline superstructure and confirm this hypothesis. Although the reason for the change of crystalline superstructure in the presence of spherical silica needs to be clarified, the reduction of the crystallization rate (or even the suppression of crystallization) of the macromolecules trapped inside the agglomerates is put forward to explain the easy deformation of the agglomerates by the growing crystallites.

Acknowledgment. This work was financially supported by Tergal Industries and the ANVAR Picardie. The stretch-blowing experiments were conducted in the Centre de Mise en Formes des Matériaux (CEMEF, Sophia-Antipolis, France). The authors thank N. Billon, E. Déloye, J.-L. Lepage, and G. Perez for their assistance and fruitful discussions. Also, the authors thank the Centre Technique des Microstructures (Université Claude Bernard-Lyon I, Lyon, France) for access to the ultramicrotomes. P. Alcouffe and J.-M. Pelletier are gratefully acknowledged for their help and advice in the field of TEM and WAXS.

References and Notes

(1) Davis, C. H.; Mathias, L. J.; Gilman, J. W.; Schraldi, D. A.; Shields, J. R.; Trulove, P.; Sutto, T. E.; Delong, H. C. *J. Polym. Sci., Part B: Polym. Phys.* **2002**, *40*, 2661−2666.

(2) Sanchez-Solis, A.; Romero-Ibarra, I.; Estrada, M. R.; Calderas, F.; Manero, O. *Polym. Eng. Sci.* **2004**, *44*, 1094−1102.

(3) Ke, Y.; Yang, Z.-B.; Zhu, C.-F. *J. Appl. Polym. Sci.* **2002**, *85*, 2677−2691.

(4) Ke, Y.; Long, C.; Qi, Z. *J. Appl. Polym. Sci.* **1999**, *71*, 1139−1146.

(5) Kim, S. H.; Park, S. H.; Kim, S. C. *Polym. Bull. (Berlin)* **2005**, *53*, 285−292.

(6) Imai, Y.; Nishimura, S.; Abe, E.; Tateyama, H.; Abiko, A.; Yamaguchi, A.; Aoyama, T.; Taguchi, H. *Chem. Mater.* **2002**, *14*, 477−479.

(7) Liu, W.; Tian, X.; Cui, P.; Li, Y.; Zheng, K.; Yang, Y. *J. Appl. Polym. Sci.* **2004**, *91*, 1229−1232.

(8) El Fray, M.; Boccaccini, A. R. *Mater. Lett.* **2005**, *59*, 2300−2304.

(9) Di Lorenzo, M. L.; Errico, M. E.; Avella, M. *J. Mater. Sci.* **2002**, *37*, 2351−2358.

(10) Qu, M.-H.; Wang, Y. Z.; Wang, C.; Ge, X. G.; Wang, D. Y.; Zhou, Q. *Eur. Polym. J.* **2005**, *41*, 2569−2574.

(11) Sekelik, J.; Stepanov, E. V.; Nazarenko, S.; Schiraldi, D.; Hiltner, A.; Baer, E. *J. Polym. Sci., Part B: Polym. Phys.* **1999**, *37*, 847−857.

(12) Lee, H.-J.; Oh, S.-J.; Choi, J.-Y.; Kim, J. W.; Han, J.; Tan, L.-S.; Baek, J.-B. *Chem. Mater.* **2005**, *17*, 5057−5064.

(13) Nevalainen, K.; MacKerron, D. H.; Kuusipalo, J. *Mater. Chem. Phys.* **2005**, *92*, 540−547.

(14) Nevalainen, K.; MacKerron, D. H.; Kuusipalo, J. *Mater. Chem. Phys.* **2007**, *101*, 103−111.

(15) Ito, K.; Nonomura, C.; Yamashita, K.; Suzuki, T.; Chinwanitcharoen, C.; Yamada, T.; Ishihara, H. *J. Appl. Polym. Sci.* **2004**, *92*, 1243−1251.

(16) Taniguchi, A.; Cakmak, M. *Polymer* **2004**, *45*, 6647−6654.

(17) Phillips, R.; Manson, J.-A. E. *J. Polym. Sci., Part B: Phys.* **1997**, *35*, 875−888.

(18) Daubeny, R. P.; Bunn, C. W. *Proc. R. Soc. London A* **1954**, *226*, 531.

(19) Bafna, A.; Beaucage, G.; Mirabella, F.; Mehta, S. *Polymer* **2003**, *44*, 1103−1115.

(20) Gantillon, B.; Spitz, R.; McKenna, T. F. *Macromol. Mater. Eng.* **2004**, *289*, 106−112.

(21) Smoluchowski, M. *Z. Phys. Chem.* **1917**, *92*, 129−168.

(22) Janssen, J. M. H. In *Materials Science and Technology*: *A Comprehensive Treatment, Processing of Polymers*; Cahn, R. W., Haasen, P., Kramer, E. J., Meijer, H. E. H., Eds.; Wiley VCH: Weinheim, 1997; Vol. 18, p 113.

(23) Gorlier, E.; Haudin, J. M.; Billion, N. *Polymer* **2001**, *42*, 9541−9549.

(24) Smith, F. S.; Steward, R. D. *Polymer* **1974**, *15*, 283−286.

(25) Gupte, K. M.; Motz, H.; Schultz, J. M. *J. Polym. Sci., Polym. Phys. Ed.* **1983**, *21*, 1927−1953.

(26) Mahendrasingam, A.; Blundell, D. J.; Martin, C.; Fuller, W.; MacKerron, D. H.; Harvie, J. L.; Oldman, R. J.; Rieke, C. *Polymer* **2000**, *41*, 7803−7814.

(27) Blundell, D. J.; Mahendrasingam, A.; Martin, W. Fuller, W.; MacKerron, D. H.; Harvie, J. L.; Oldman, R. J.; Rieke, C. *Polymer* **2000**, *41*, 7793−7802.

(28) Le Bouvellec, G.; Monnerie, L.; Jarriy, J.-P. *Polymer* **1986,** *27*, 856−860.

(29) Boyaud, M. F.; Aït-Kadi, A.; Bousmina, M.; Michel, A.; Casagnau, P. *Polymer* **2001**, *42*, 6515−6526.

(30) Fenouillot, F.; Perier-Camby, H. *Polym. Eng. Sci.* **2004**, *44*, 625−637.

(31) Hu, Y. S.; Prattipati, V.; Mehta, S.; Schiraldi, D. A.; Hiltner, A.; Baer, E. *Polymer* **2005**, *46*, 2685−2698.

(32) Li, L.; de Jeu, W. H. *Adv. Polym. Sci.* **2005**, *181*, 75−120.

(33) Somani, R. H.; Yang, L.; Zhu, L.; Hsiao, B. H. *Polymer* **2005**, *46*, 8587−8623.

(34) Blundell, D. J.; MacKerron, D. H.; Fuller, W.; Mahendrasingam, A.; Martin, C.; Oldman, R. J.; Rule, R. J.; Riekel, C. *Polymer* **1996**, *37*, 3303−3311.

(35) Welsh, G. E.; Blundell, D. J.; Windle, A. H. *Macromolecules* **1998**, *31*, 7562−7565.

(36) Mahendrasingam, A.; Martin, C.; Fuller, W.; Blundell, D. J.; Oldman, R. J.; Harvie, J. L.; MacKerron, D. H.; Rieke, C.; Engström, P. *Polymer* **1999**, *40*, 5553−5565.

(37) Mahendrasingam, A.; Martin, C.; Fuller, W.; Blundell, D. J.; Oldman, R. J.; MacKerron, D. H.; Harvie, J. L.; Rieke, C. *Polymer* **2000**, *41*, 1217−1221.

(38) Welsh, G. E.; Blundell, D. J.; Windle, A. H. *J. Mater. Sci.* **2000**, *35*, 5225−5240.

(39) Kawakami, D.; Hsiao, B. S.; Burger, C.; Ran, S.; Avila-Orta, C.; Sics, I.; Kikutani, T.; Jacob, K. I.; Chu, B. *Macromolecules* **2005**, *38*, 91−103.

(40) Kawakami, D.; Ran, S.; Burger, C.; Avila-Orta, C.; Sics, I.; Chu, B.; Hsiao, B. S.; Kikutani, T. *Macromolecules* **2006**, *39*, 2909−2920.

(41) Murthy, N. S.; Grubb, D. T.; Zero, K.; Nelson, C. J.; Chen, G. *J. Appl. Polym. Sci.* **1998**, *70*, 2527−2538.

(42) Mahendrasingama, A.; Blundell, D. J.; Martin, C.; Fuller, W.; MacKerron, D. H.; Harvie, J. L.; Oldman, R. J.; Rieke, C. *Polymer* **2000**, *41*, 7803−7814.

(43) Asano, T.; Balta, Calleja, F. J.; Flores, A.; Tanigaki, M.; Mina, M. F.; Sawatari, C.; Itagaki, H.; Takahashi, H.; Hatta, I. *Polymer* **1999**, *40*, 6475−6484.

(44) Hsiao, B. S.; Yang, L.; Somani, R. H.; Avila-Orta, C. A.; Zhu, L. *Phys. Rev. Lett.* **2005**, *94*, 117802.

(45) Li, L.; de Jeu, W. H. *Macromolecules* **2004**, *37*, 5646−5652.

(46) Yoshioka, T.; Tsuji, M.; Kawahara, Y.; Kohjiya, S.; Manabe, N.; Yokota, Y. *Polymer* **2005**, *46*, 4987−4990.

(47) Yoshioka, T.; Tsuji, M.; Kawahara, Y.; Kohjiya, S. *Polymer* **2003**, *44*, 7997−8003.

(48) Haubruge, H. G.; Jonas, A. M.; Legras, R. *Macromolecules* **2004**, *37*, 126−134.

(49) Waddon, A. J.; Petrovic, Z. S. *Polym. J.* **2002**, *34*, 876−881.

(50) Nitta, K.; Asuka, K.; Liu, B.; Terano, M. *Polymer* **2006**, *47*, 6457−6463.

MA062886I